One-mode Ginzburg-Landau theory of surface energy anisotropy

Chih-Chun Wang and Kuo-An Wu*
Department of Physics, National Tsing Hua University, 30013 Hsinchu, Taiwan

(Received 16 December 2022; accepted 27 March 2023; published 4 April 2023)

It is well established that for diffusive solid-liquid interfaces the interfacial anisotropy arises due to symmetry breaking of density waves at the interface. While the interfacial anisotropy is expected to be related to the underlying lattice symmetry, the anisotropy can still differ among materials with the same lattice structure due to the difference in the interatomic potentials. To shed light on this, a general Ginzburg-Landau (GL) theory of solid-liquid interfaces, based on crystal symmetry and classical density functional theory, is proposed to analytically connect the relation between lattice symmetry, the shape of the free-energy landscape, and surface energy anisotropy. Using a perturbative scheme, we show that the corresponding anisotropic form of the surface energy, depending on crystal symmetry, naturally appears in the perturbation expansion. To explore how the double-well free-energy landscape in the GL theory affects the anisotropy, we consider lattices of hexagonal symmetry as an example, for which the shape of the free-energy landscape is shown to only depend on one parameter. The dependence of anisotropy on the free-energy landscape predicted by the perturbation scheme is shown to be in good agreement with numerical solutions of the GL theory. Finally, a universal relation between density wave profile widths and the anisotropy parameter of the surface energy is proposed and validated using a phase-field crystal method.

DOI: 10.1103/PhysRevB.107.144101

I. INTRODUCTION

Surface energy refers to the excess free energy associated with the presence of an interface [1]. In a system where solid and liquid coexist, the interfacial energy possesses an angular dependence with respect to the orientation of the lattice due to the discrete rotational symmetry of crystal lattices. This anisotropy plays a crucial role in complex morphology of crystal growth during solidification [2–5], as shown in phase-field simulations [6–12], and the resulting microstructures determine greatly the properties of materials at the macroscopic level. The anisotropy, though material dependent, is shown to strongly depend on the crystal structure [13–18], which suggests that a plausible way of understanding the physical origin of anisotropy is through continuum theories involving density waves of the corresponding crystal symmetry.

The Ginzburg-Landau (GL) theory, which employs the amplitudes of density waves corresponding to the principal reciprocal lattice vectors (RLVs) as order parameters, has been used to illustrate successfully the relation between the surface anisotropy and underlying crystal symmetry [19–22]. The GL theory for a solid-liquid system at equilibrium has its roots in the classical density functional theory (DFT) of freezing [23–27], from which it is derived by treating the solid as a perturbed liquid with specified crystal symmetry. With the input of the direct correlation function (DCF) of the liquid (or, equivalently, the liquid structure factor) from molecular dynamics (MD) simulations, the GL theory has been shown to make good quantitative predictions as to the interface width, density wave profiles across the interface, and surface anisotropies [20,28]. Regardless of these successes, it is of interest to note that in spite of the simplistic form of the GL theory, the density waves still couple with each other nonlinearly, making it less analytically tractable. As a consequence, the density wave profiles across the interface as well as the anisotropy are commonly obtained numerically, and the anisotropic form of the surface energy is usually presumed rather than derived. In addition, it is shown in the GL theory and phase-field crystal (PFC) simulations that the anisotropy also depends on the nonlinear interactions among density waves [19–21,29–35].

Specifically, Wu *et al.* have obtained the comparable anisotropy and density wave profiles at various crystal faces for the body-centered cubic (bcc) solid-liquid interface with a first-mode GL theory [20]. There, the coefficients of the squared-gradient terms and the double-well potential in the free energy are derived directly from classical DFT and are expressed in terms of the DCF. Majaniemi and Provatas [21] considered a GL theory for the hexagonal and bcc lattices. With a hyperbolic tangent ansatz, they obtained expressions for the interface width and the interfacial energy. Furthermore, it is argued, via the observation that γ is proportional to the sum of the directional cosine squared, that $\gamma(\theta)$ for the hexagonal lattice is a power series of $\cos 6\theta$, to which simulation results are fitted. Similarly, albeit with PFC as the starting point, Ofori-Opoku *et al.* [36] obtained an effective free-energy functional of the PFC amplitudes, with the formula for $\gamma(\theta)$ ultimately relying on the knowledge of the anisotropic profiles of the amplitudes. Meanwhile, the information of anisotropy near the critical point $\epsilon = 0$ of the

*kuoan@phys.nthu.edu.tw

PFC is examined in detail by Tóth and Provatas, who showed that in said regime the principal mode amplitudes' critical exponent is strictly smaller than those of the remaining modes, and hence the principal modes dominate the RLV expansion [22]. The derived interfacial energy depends on the envelope function, which is assumed to take the form of the hyperbolic tangent function. Despite these previous efforts, exactly how the interaction between density waves affects the anisotropy remains unclear, and a more analytically tractable approach is needed to answer this question.

To shed light on the above issues, we present in this paper a general framework of forming a free-energy functional for the GL theory based on lattice symmetry and classical DFT. A perturbative scheme is then introduced to explore the emergence of the surface energy anisotropy analytically. Specifically, we show that the n-fold anisotropy of two-dimensional (2D) crystals and the cubic anisotropy of the face-centered-cubic (fcc) crystals appear naturally in the perturbation expansion. In addition, taking the 2D hexagonal lattice as an example, we show explicitly how the anisotropy changes with the shape of the free-energy landscape, which dictates the interaction among density waves. Since the free-energy landscape uniquely determines the density wave profiles and anisotropy, a universal relation among dimensionless quantities such as the ratio of profile widths and anisotropy is expected. Such relation is examined using a generalized PFC model, whose results are shown to be in good agreement with the GL theory quantitatively.

The paper is organized as follows. In Sec. II, a GL theory based on the classical DFT of freezing is reviewed. By scaling out the material-dependent DCF, the dimensionless GL free-energy functional could only differ in the shape of the local free energy, which gives rise to different values of anisotropy. In Sec. III, the parametrization of the double-well-shaped free-energy landscape for various lattice symmetries is discussed. To explicitly show how the free-energy landscape changes the surface energy anisotropy, the GL theory is solved numerically for 2D hexagonal lattices. In Sec. IV, a perturbative scheme is presented to analytically connect crystal symmetry, free-energy landscape, and surface energy anisotropy. Finally, the universal relation between the width ratio and anisotropy predicted by the GL theory is validated using a generalized PFC model in Sec. V.

II. ORDER PARAMETER MODEL OF LIQUID-SOLID SYSTEMS AT EQUILIBRIUM

The derivation of the classical density functional theory of freezing was outlined by Ramakrishnan and Yussouff in 1979 [23]. The theoretical framework is able to explain a wide range of phenomena regarding the liquid state using only the information of the static structure factor $S(k)$ or, equivalently, the DCF $C(k)$. The free-energy functional can be cast into the simple form [24]

$$\frac{\Delta\Omega[\rho(\mathbf{r})]}{k_BT} = V\rho_l + \int d\mathbf{r}\,[\rho_l + \Delta\rho(\mathbf{r})]\left[\ln\left(1+\frac{\Delta\rho(\mathbf{r})}{\rho_l}\right)\right] - \frac{1}{2}\int d\mathbf{r}d\mathbf{r}'\Delta\rho(\mathbf{r})C(|\mathbf{r}-\mathbf{r}'|)\Delta\rho(\mathbf{r}'), \quad (1)$$

which is a functional of the density difference $\Delta\rho(\mathbf{r})$ relative to the liquid density ρ_l.

To study a system involving liquid-solid coexistence with known underlying lattice structures, it is a common practice to employ an ansatz for the density that is composed of density waves with corresponding reciprocal lattice vectors. The physical properties of a liquid-solid system can then be expressed in terms of the spatially varying amplitudes of density waves across the liquid-solid interface. That is, the local density of the system $\rho(\mathbf{r})$ can be written as [19–21,24,37–39]

$$\rho(\mathbf{r}) = \rho_l\left[u_0(\mathbf{r}) + \sum_{i=1}^{\mathcal{N}} u_i(\mathbf{r})e^{i\mathbf{k}_i\cdot\mathbf{r}}\right], \quad (2)$$

where ρ_l is the liquid density, $\rho_l u_0(\mathbf{r})$ is the local mean density, u_i are the amplitudes of the density wave of wave vector $\mathbf{k}_i$, and $\mathcal{N}$ is the total number of reciprocal lattice vectors taken into account. The liquid state corresponds to $u_0(\mathbf{r}) = 1$ and vanishing u_i's. On the other hand, a homogeneous solid of density ρ_s occurs with a fixed set of *constant* $u_i(\mathbf{r}) = u_s$, and $\rho_l u_0(\mathbf{r}) = \rho_s$. A liquid-solid coexistent system can then be described by position-dependent u_i's and u_0. With the ansatz above, Haymet and Oxtoby employed classical DFT to investigate interfacial properties, such as the surface energy and the shapes of the density profiles [24,25,40]. However, in order to obtain converging results, this calculation is computationally intensive since hundreds of reciprocal lattice vectors are required. On the other hand, anisotropy of interfacial properties of liquid-solid systems is shown to be closely related to the lattice symmetry, which suggests that few reciprocal lattice vectors are sufficient to describe the interfacial anisotropy [20,41]. In addition, as shown by Shih *et al.*, the effect of the mean density difference between the solid and liquid on the surface energy can be implicitly included by renormalizing coefficients of u_i's in the free-energy functional [19]. Hence a constant mean density $u_0(\mathbf{r}) = 1$ is assumed, and only amplitudes of principal reciprocal lattice vectors are employed for the following discussion. That is, $\rho(\mathbf{r}) = \rho_l(1 + \sum_{i=1}^{2N} u_i(\mathbf{r})e^{i\mathbf{k}_i\cdot\mathbf{r}})$, with $2N$ being the number of principal RLVs. Furthermore, for diffusive interfaces, a more analytical tractable approach is to expand the nonlocal correlation function in Eq. (1) around $\mathbf{r}$ up to the quadratic term, and one can rewrite the spatial correlation term as a squared-gradient term [20,28]. Terms consisting of higher-order derivatives, such as $\partial^2 u^* \partial^2 u$, can be included to account for scale coupling in the case of thin interfaces [42,43]. However, since we focus mainly on diffusive interfaces, where the scale on which $u_i(\mathbf{r})$ vary is much larger than the RLV scale (i.e., that of $\mathbf{k}_i$), such terms are dropped. The grand potential difference with respect to a homogeneous reference liquid system is then written as

$$\frac{\Delta\Omega[\rho(\mathbf{r})]}{\rho_l k_B T/2} = \int d\mathbf{r}\left[-\frac{1}{2}\sum_{i=1}^{2N} C''(k)\frac{k_i^\mu k_i^\nu}{k^2}\partial_\mu u_i^* \partial_\nu u_i + U(\mathbf{u})\right], \quad (3)$$

where $k \equiv |\mathbf{k}_i|$, $U(\mathbf{u})$ is a double-well potential with two minima at $u_i = 0$ and $u_i = u_s$ corresponding to liquid and solid states, respectively, and $\mathbf{u}$ represents the set of u_i's. Moreover, from the classical DFT of freezing, the coefficient of each of the quadratic terms $|u_i|^2$ in $U(\mathbf{u})$ is equal to $1/S(k)$. To

formulate a more generalized expression that depends only on the lattice symmetry but not on individual materials, the fields are rescaled by defining $\psi_i \equiv u_i/|u_s|$ so that $\psi_i = 0$ and $\psi_i = 1$ correspond to the liquid and solid states. In addition, the material-dependent factors, $-C''(k)$ and $S(k)$, are eliminated by rescaling the length and the free energy so that the generalized form only depends on the lattice symmetry. We obtain the dimensionless Ginzburg-Landau-type free energy,

$$\Delta\mathcal{F} = \int d\boldsymbol{\xi}\left[\frac{1}{2}\sum_{i=1}^{2N}\hat{k}_i^{\mu}\hat{k}_i^{\nu}\partial_{\xi}^{\mu}\psi_i^{*}\partial_{\xi}^{\nu}\psi_i + V(\boldsymbol{\psi})\right], \tag{4}$$

where $\hat{k}_i^{\mu} \equiv k_i^{\mu}/k$, $\boldsymbol{\xi} \equiv \mathbf{r}/\sqrt{-S(k)C''(k)/2} \equiv \mathbf{r}/\lambda$, and $\Delta\mathcal{F} \equiv \Delta\Omega \cdot S(k)\lambda^{2-d}/(|u_s|^2\rho_l k_B T)$ with d being the number of spatial dimensions, and the rescaled potential is $V(\boldsymbol{\psi}) \equiv U(\boldsymbol{\psi}) \cdot S(k)/(2|u_s|^2)$, for which $\partial^2 V/\partial\psi_i\partial\psi_i^* = 1/2$. With a given lattice symmetry, the variation of $V(\boldsymbol{\psi})$ alone could result in different values of the surface energy anisotropy, which may explain the different anisotropies seen for materials with the same lattice structure.

In this paper, the generalized expression is used to explore how the lattice symmetry as well as the shape of the potential affect the interfacial energy anisotropy of liquid-solid interfaces. For a planar liquid-solid interface with its normal $\hat{\mathbf{n}}$ aligned to $\hat{\boldsymbol{\xi}}_{\perp}$, the interfacial energy, defined as the excess free energy per surface area, is simply

$$\gamma \equiv \Delta\mathcal{F}\Big/\int d\boldsymbol{\xi}_{\parallel} = \int d\xi_{\perp}\left[\frac{1}{2}\sum_{i=1}^{2N}c_i^2|\partial_{\xi_{\perp}}\psi_i|^2 + V(\boldsymbol{\psi})\right], \tag{5}$$

where $\boldsymbol{\xi}_{\parallel}$ are dimensionless coordinates parallel to the interface. Since the above expression is, for planar liquid-solid interfaces, only dependent on $\xi_{\perp}$, hereafter we define $\xi \equiv \xi_{\perp}$ and $\partial \equiv \partial_{\xi} \equiv \partial_{\xi_{\perp}}$ for simplicity.

The factors $c_i \equiv \hat{\mathbf{k}}_i \cdot \hat{\mathbf{n}}$ in Eq. (5) are the squared-gradient coefficients and in two dimensions can be parametrized by an angle θ so that $\hat{\mathbf{n}} = \hat{\mathbf{x}}\cos\theta + \hat{\mathbf{y}}\sin\theta$ and $c_i^2 = \cos^2(\theta - \theta_i)$ with a fixed set of $\hat{\mathbf{k}}_i = \hat{\mathbf{x}}\cos\theta_i + \hat{\mathbf{y}}\sin\theta_i$. The orientation-dependent squared-gradient coefficients have been shown to be responsible for the anisotropy of interfacial energy. In this paper, we present an analytical investigation to shed light on how the orientation-dependent squared-gradient coefficients lead to interfacial anisotropy and how couplings between density waves could also affect the anisotropy of the surface energy.

III. LATTICE SYMMETRY, POTENTIAL, AND SURFACE ENERGY ANISOTROPY

It is established that the interfacial anisotropy arises due to symmetry breaking of density waves at the interface [3,19,20,25,28]. Therefore the interfacial anisotropy is expected to be universally related to the underlying lattice symmetry. However, the details and the magnitude of anisotropy can still differ among materials with the same lattice structure due to variations in density wave profiles as a result of the difference in the interatomic potentials. In this section, we present quantitative results of equilibrium liquid-solid interfaces with different forms of potentials using numerical simulations, in particular the anisotropic amplitude profiles $\psi_i(\xi)$ and interfacial energy $\gamma(\theta)$. Additionally, an analytical perturbative framework is presented to elucidate the relation between the lattice symmetry and the surface energy anisotropy as well as the dependence of the anisotropy on the potential $V(\boldsymbol{\psi})$.

It is clear that the exact form of $V(\boldsymbol{\psi})$ is not unique given that $V(\boldsymbol{\psi})$ is of the form of a double well. Nevertheless, the general form of the double-well potential is constrained by the requirement of obeying the lattice symmetry while comprising two local minima having the same energy. Take a two-dimensional square lattice as an example: Since the amplitudes for $+\mathbf{k}_i$ and $-\mathbf{k}_i$ are complex conjugates, there are only two independent complex density amplitudes required to describe the liquid-solid system. However, when the lattice distortion across the liquid-solid interface is small [25,44], the phases of complex density amplitudes are approximately constants. It follows that by a shift of the origin of the coordinate system, one can make these phases vanish such that two *real* density amplitudes, ψ_1 and ψ_2, are sufficient to describe a square-liquid coexistence system. With these two amplitudes, for a square lattice, the simplest potential is a combination of sextic, quartic, and quadratic terms that obey the point-group symmetry and can be conveniently parametrized by two parameters, κ and κ' (see Appendix A for a detailed discussion):

$$\begin{aligned} V(\psi_1,\psi_2) = {} & \psi_1^6 - 2\psi_1^4 + \psi_1^2 + \psi_2^6 - 2\psi_2^4 + \psi_2^2 \\ & + \kappa\left(\psi_1^4 + \psi_2^4 - 2\psi_1^2\psi_2^2\right) \\ & + \kappa'\left(\psi_1^6 + \psi_2^6 - \psi_1^4\psi_2^2 - \psi_1^2\psi_2^4\right). \end{aligned} \tag{6}$$

The reason for which κ and κ' are the only two degrees of freedom for the generalized potential of the square lattice is briefly stated as follows. There are a total of five terms obeying both the point-group symmetry of the square lattice, which requires V to be invariant under permutation of ψ_1 and ψ_2, and translational invariance, which dictates that only terms whose wave vectors sum to zero are allowed in $V(\boldsymbol{\psi})$. These are $\psi_1^2 + \psi_2^2$, $\psi_1^4 + \psi_2^4$, $\psi_1^2\psi_2^2$, $\psi_1^6 + \psi_2^6$, and $\psi_1^4\psi_2^2 + \psi_1^2\psi_2^4$. These terms as well as their first derivatives automatically vanish at the liquid well, i.e., when $\psi_1 = \psi_2 = 0$, which are two of the constraints for a double-well potential. However, three constraints, (a) that V admit a local minimum at the solid well, where $\psi_1 = \psi_2 = 1$, (b) that the solid and liquid wells be balanced, i.e., $V(\psi_1 = \psi_2 = 0) = V(\psi_1 = \psi_2 = 1)$, and (c) that the quadratic coefficient be unity, leave the system with $5 - 3 = 2$ independent parameters, namely, κ and κ'. For other relevant lattice structures such as hexagonal and fcc lattices, the symmetry operations and the generalized potentials are discussed in detail in Appendix A.

Since the amplitudes ψ_i are real, as in Eq. (5), the free energy per unit surface area for a planar liquid-solid system can be rewritten as

$$\gamma = \int d\xi\left[\sum_{i=1}^{N}c_i^2(\partial\psi_i)^2 + V(\psi)\right], \tag{7}$$

where the summation from 1 to N now ensures that only one of $\mathbf{k}_i$ and $-\mathbf{k}_i$ is included. The equilibrium amplitude profiles of liquid-solid coexistence are then obtained by relaxing the

fields $\psi_i(\mathbf{r})$ towards the minimum of Eq. (7):

$$\frac{\partial \psi_i}{\partial t} = -\frac{\delta \gamma}{\delta \psi_i} = 2c_i^2 \partial^2 \psi_i - \frac{\partial V}{\partial \psi_i}. \tag{8}$$

In this section, we focus on the interfacial energy of the hexagonal lattice in two dimensions for which the simplest double-well potential is only quartic and consists of solely one free parameter κ. Namely,

$$V(\boldsymbol{\psi}) = \sum_{i=1}^{3} \left(\psi_i^4 + \psi_i^2\right) - 6\psi_1\psi_2\psi_3 + \kappa\left(\psi_1^4 + \psi_2^4 + \psi_3^4 - \psi_1^2\psi_2^2 - \psi_1^2\psi_3^2 - \psi_2^2\psi_3^2\right). \tag{9}$$

With the principal reciprocal lattice vectors $\mathbf{k}_i$ remaining fixed at $\theta_i = (0, 2\pi/3, 4\pi/3)$, for a planar interface with its normal specified by the angle θ, the squared-gradient coefficients are given by $c_i^2 = \cos^2(\theta - 2(i-1)\pi/3)$.

The angular dependence of the squared-gradient coefficients $c_i^2(\theta)$ leads to an anisotropic interfacial energy $\gamma(\theta)$ which is crucial to understanding the surface morphology in a wide range of physical systems. We follow the convention used in Refs. [22,45] and define the anisotropy parameter α_γ for the interfacial energy as

$$\alpha_\gamma \equiv \frac{\gamma(0^\circ) - \gamma(30^\circ)}{\gamma(0^\circ) + \gamma(30^\circ)}. \tag{10}$$

Figure 1 shows that both the anisotropy parameter α_γ and the mean value of γ vary with the shape of the potential, which is parametrized by κ. To quantify the change in the magnitude of γ, we define the energy offset $\Delta\overline{\gamma}$ as the energy drop compared with that of the isotropic system, which will be shown to be equal to $\sqrt{2}/2$ for hexagonal lattices in later discussions within this section. It is apparent that α_γ and the energy offset decrease as κ is increased. This can be understood by considering the following picture: As κ becomes larger, the energy landscape penalizes more the deviations among density amplitudes across the interface since the last term in Eq. (9) can be rewritten as $V_{\text{coupling}} = \frac{\kappa}{2}\sum_{i\neq j}(\psi_i - \psi_j)^2$. Taking into account that if all amplitudes were identical, the interfacial energy would be simply proportional to $\sum c_i^2$, which is independent of θ, it is then natural to argue that the angular dependence of γ is weakened as amplitude-amplitude coupling gets stronger. Similarly, the energy offset diminishes as κ increases since the system becomes more isotropic. Figure 2 plots the amplitude profiles across interfaces at $\theta = 0$ and $\theta = \pi/6$, respectively. It shows that amplitude profiles behave more isotropically as the coupling strength κ gets stronger. It is also worth noting that with $\kappa = -1$ the anisotropy parameter $\alpha_\gamma \approx 0.23\%$ is close to the PFC result for $\epsilon = 0.1$ as reported in Ref. [45]. The corresponding polar plot of the interface stiffness is shown in Fig. 1(c). The connection between the present theory and the PFC model will be discussed in Sec. V.

In principle, since the form of the potential arises due to only the symmetry argument, it is possible to express potential parameters in terms of physical parameters employed in the classical DFT of freezing. Nevertheless, the theory in its dimensionless form, i.e., the free-energy functional on the right-hand side of Eq. (7), does not lack predictive power at all if the anisotropy parameter α_γ is related to other dimensionless quantities, such as the ratio of profile widths, as we will see in the next section.

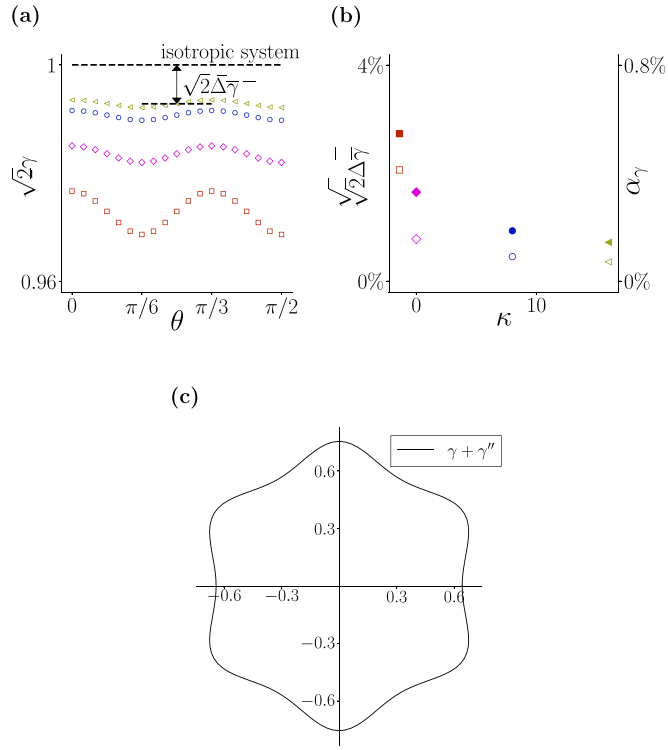

FIG. 1. (a) $\gamma(\theta)$ obtained with simulations with $\kappa = -1.4$, 0, 8, and 16 (from bottom to top). (b) The corresponding energy offsets (solid symbols) and anisotropies (open symbols) plotted against the coupling parameter κ. (c) A polar plot of interface stiffness, $\gamma + d^2\gamma/d\theta^2$, for $\kappa = -1$, which corresponds to $\alpha_\gamma = 0.23\%$.

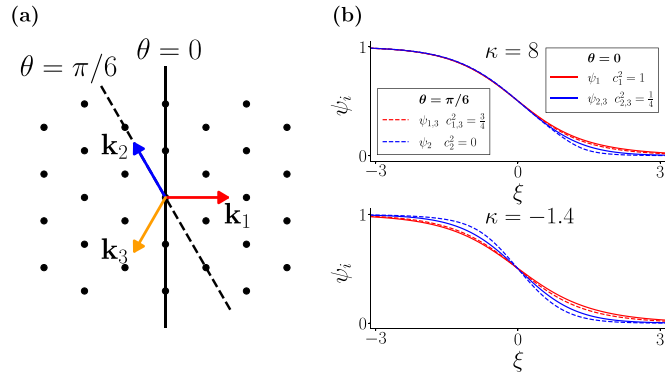

FIG. 2. (a) The principal reciprocal lattice vectors of the hexagonal lattice along with two planar interfaces, showing the interface orientations relative to the principal RLVs. (b) Simulated density profiles at different κ. Solid lines represent profiles at interfacial angle $\theta = 0$, and dashed lines correspond to $\theta = \pi/6$, as indicated in (a).

IV. PERTURBATION THEORY

As stated in the Introduction, in previous studies, this type of double-well system has been either solved by numerical methods or analyzed with a reasonable yet arbitrary ansatz for the profiles (e.g., the tanh function), largely due to mathematical difficulties in solving nonlinear coupled equations analytically. While the numerical solutions are shown to successfully relate the interfacial anisotropy to the underlying lattice symmetry once the potential is specified, a quantitative relationship between the form of the potential and the anisotropy is yet to be encountered. Therefore a perturbative method is proposed here to yield approximate analytical solutions to the aforementioned model [i.e., Eq. (7)], which provides a guide that connects the details of the potential to the interfacial properties.

A. Isotropic system and squared-gradient perturbations

We start by considering an isotropic system as our reference system where every squared-gradient coefficient takes the same value, chosen to be $\langle c_i^2\rangle = 1/d$, with d being the number of spatial dimensions. The free energy is then isotropic and takes the form

$$\gamma_0 \equiv \int d\xi \left[\sum_{i=1}^{N} \frac{1}{d}(\partial\psi_i)^2 + V(\psi)\right], \tag{11}$$

which is minimized by the isotropic density profiles denoted by $\psi_i^{(0)}$. Owing to the symmetry constraint, it is evident that at least one set of solutions exists and it is $\psi_1^{(0)} = \cdots = \psi_N^{(0)} \equiv \psi^{(0)}(\xi)$. For a general θ, the squared-gradient coefficients differ from each other, giving rise to anisotropy in interfacial properties [22,36]. With the isotropic solutions as unperturbed states, the corrections to amplitude profiles are then solved by treating the anisotropic part as perturbations. In particular, the free-energy functional is separated into the unperturbed isotropic part and a perturbation term, which consists of squares of derivatives of each field with anisotropic squared-gradient coefficients:

$$\gamma = \gamma_0 + \gamma_1 = \gamma_0 + \int d\xi \sum_{i=1}^{N}\left(c_i^2 - \frac{1}{d}\right)(\partial\psi_i)^2. \tag{12}$$

It is worth noting that the isotropic system should be seen as a mathematical device that arises when one looks for an appropriate unperturbed system that is solvable, and need not correspond to any real physical configuration of the system. Of course, in the case of the square lattice, this is achievable by setting $\theta = \pi/4$ so that $c_1^2 = c_2^2 = 1/2$. However, for the hexagonal lattice, where the squared-gradient coefficients are chosen so that the sixfold symmetry generated by the underlying hexagonal lattice is respected, no orientations of the lattice correspond to the ideally isotropic system. That is, such a functional is no longer physically possible.

B. Perturbative solutions to γ and $\psi_i(\xi)$

Cast into the form in Eq. (12), the interfacial energy γ, along with the density amplitudes $\psi_i(\xi)$, can then be computed order by order with the use of the general functional perturbation theory outlined in Appendix B. One immediate consequence is that, since $\sum_i (c_i^2 - 1/d) = 0$, the first-order energy correction given by $\gamma^{(1)} = \gamma_1[\boldsymbol{\psi}^{(0)}(\xi)]$ vanishes, that is, $\gamma^{(1)} = 0$. On the other hand, the equation of motion at $O(\epsilon^1)$ gives the governing equation of $\psi_i^{(1)}$:

$$\Delta_{ij}^2\gamma_0 \cdot \psi_j^{(1)} + \Delta_i\gamma_1 = 0, \tag{13}$$

where repeated indices are summed over and Δ_{ij}^2 and Δ_i represent functional derivatives with respect to the fields ψ_i (see Appendix B for details). The first term in Eq. (13) involves an operator $\Delta_{ij}^2\gamma_0$ acting on the first-order fields, which is expressed explicitly as

$$\Delta_{ij}^2\gamma_0 \cdot \psi_j^{(1)}(\xi) = \left[-\frac{2}{d}\delta_{ij}\partial^2 + \frac{\partial^2 V}{\partial\psi_i\partial\psi_j}\right]\psi_j^{(1)}, \tag{14}$$

where the second term in the parentheses is evaluated at $\boldsymbol{\psi}^{(0)}$. Here, we define two operators which will facilitate our calculations later when we Fourier-transform the fields with respect to the field indices. These are

$$\hat{D} \equiv -\frac{2}{d}\partial^2 + \frac{\partial^2 V}{\partial\psi_i^2},$$
$$\hat{C} \equiv \frac{\partial^2 V}{\partial\psi_i\partial\psi_j}. \tag{15}$$

Although the action of $\hat{C}$ on a function f is just a multiplication of functions, we still denote it as an operator. Meanwhile, the second term in Eq. (13) is the anisotropic deviation of the squared-gradient coefficients multiplied by the second derivative of the fields evaluated at $\boldsymbol{\psi}^{(0)}$. Equation (13) then takes the form

$$(\hat{D}\delta_{ij} + \hat{C}\delta_{i\neq j})\psi_j^{(1)} = \frac{2}{d}\sigma_i\partial^2\psi^{(0)}, \tag{16}$$

where $\sigma_i \equiv dc_i^2 - 1$. Note that for square, hexagonal, and fcc lattices, due to the symmetry constraints for the potential, both $\hat{D}$ and $\hat{C}$ are independent of the choice of ψ's in evaluating $\partial^2 V/\partial\psi_i\partial\psi_j$. Therefore the left-hand side of Eq. (16) is symmetric under permutations of field indices, allowing one to take a Fourier-like transform of the fields as

$$\tilde{\psi}_n \equiv \sum_{k=1}^{N}(e^{2\pi i/N})^{nk}\ \psi_k. \tag{17}$$

The transformation decouples Eq. (16) into N independent equations. We obtain

$$[\hat{D} + (N-1)\hat{C}]\tilde{\psi}_0^{(1)} = \tilde{\sigma}_0\partial^2\psi^{(0)} = 0, \tag{18a}$$
$$(\hat{D} - \hat{C})\tilde{\psi}_{n\neq 0}^{(1)} = \tilde{\sigma}_n\partial^2\psi^{(0)}. \tag{18b}$$

The invariance of the functional $\gamma[\boldsymbol{\psi}(\xi)]$ under $\boldsymbol{\psi}(\xi) \to \boldsymbol{\psi}(\xi + \zeta)$ means that the profile corrections $\psi_i^{(1)}(\xi)$ are not unique, and is manifest in the singularity of $\hat{D} + (N-1)\hat{C}$. The ambiguity is cured when the translational invariance is explicitly broken via the requirement that $\psi_i^{(1)}(\xi = 0) = 0$. That is, we prevent the unperturbed solution $\psi^{(0)}(\xi)$ from being corrected in such a manner that the result is merely a pure spatial translation. This condition together with Eq. (18a) conveniently leads to $\tilde{\psi}_0^{(1)}(\xi) = 0$. $\tilde{\psi}_{n\neq 0}^{(1)}$ is then solved by inverting the kernel $(\hat{D} - \hat{C})$, yielding

$\tilde{\psi}_n^{(1)} = \tilde{\sigma}_n(\hat{D}-\hat{C})^{-1}\partial^2\psi^{(0)}$, or, defining $\hat{K} \equiv \hat{D}-\hat{C}$ and taking the inverse Fourier transform,

$$\psi_i^{(1)} = \sigma_i \hat{K}^{-1}\partial^2\psi^{(0)}. \tag{19}$$

Before proceeding further, it is convenient to introduce the notation for the inner product defined as $\langle f|g\rangle \equiv \int d\xi\ f(\xi)g(\xi)$. The second-order energy consequently takes a rather concise form:

$$\gamma^{(2)} = \frac{1}{2}\Delta_i\gamma_1 \cdot \psi_i^{(1)} = -\frac{1}{2}\left(\sum_i \sigma_i^2\right)\langle\psi^{(0)}|\partial^2\hat{K}^{-1}\partial^2|\psi^{(0)}\rangle\,. \tag{20}$$

The factor $\sum\sigma_i^2$ depends on the lattice structure in question:

$$\sum_i \sigma_i^2 = \begin{cases} 1+\cos 4\theta & \text{(square)} \\ \frac{3}{2} & \text{(hexagonal)} \\ \frac{16}{5}\left[1-\frac{2}{\sqrt{21}}K_{4,1}(\theta,\varphi)\right] & \text{(fcc),} \end{cases} \tag{21}$$

where the cubic harmonic $K_{4,1}$ is as defined in Ref. [46]. It is clear that for square and fcc lattices, said factor contributes to $\gamma^{(2)}$ a harmonic angular dependence reflecting the corresponding symmetry. Whereas in the case of hexagonal lattices, the second-order energy correction is independent of θ, and the information of anisotropy is contained only in $\gamma^{(3)}$ and above.

The third-order energy correction, as derived in Appendix B, is

$$\gamma^{(3)} = \tfrac{1}{6}\Delta_{ijk}^3\gamma_0 \cdot \psi_i^{(1)}\psi_j^{(1)}\psi_k^{(1)} + \tfrac{1}{2}\Delta_{ij}^2\gamma_1 \cdot \psi_i^{(1)}\psi_j^{(1)}. \tag{22}$$

Substituting in the forms of γ_0 and γ_1 given by Eq. (12) yields the resulting third-order correction:

$$\begin{aligned}\gamma^{(3)} &= -\frac{1}{4}\left(\sum_i \sigma_i^3\right)\langle\psi^{(0)}|\partial^2\hat{K}^{-1}\partial^2\hat{K}^{-1}\partial^2|\psi^{(0)}\rangle \\ &\quad + \frac{1}{6}\sigma_i\sigma_j\sigma_k\,\langle\psi^{(0)}|\partial^2\hat{K}^{-1}\frac{\partial^3 V}{\partial\psi_i\partial\psi_j\partial\psi_k}[\hat{K}^{-1}\partial^2\psi^{(0)}]^2\rangle \\ &\equiv \left(\sum_i \sigma_i^3\right)\mathcal{G} + \sigma_i\sigma_j\sigma_k\mathcal{G}_{ijk}. \end{aligned} \tag{23}$$

We now show that $\gamma^{(3)} \propto \cos 6\theta$ for hexagonal lattices: Since the coefficients $\mathcal{G}_{ijk}$ are completely symmetric with respect to the indices, the second term of the last line in Eq. (23) can be written as

$$\left(\sum_i \sigma_i^3\right)\mathcal{G}_{111} + 3\left(\sum_{\text{sym}} \sigma_1^2\sigma_2\right)\mathcal{G}_{112} + 6\sigma_1\sigma_2\sigma_3\mathcal{G}_{123}. \tag{24}$$

The symmetric polynomials of σ_i that appear in the above expression are all proportional to $\cos 6\theta$: $\sum\sigma_i^3 = \frac{3}{4}\cos 6\theta$, $\sum_{\text{sym}}\sigma_1^2\sigma_2 = -\frac{3}{4}\cos 6\theta$, and $\sigma_1\sigma_2\sigma_3 = \frac{1}{4}\cos 6\theta$. It follows that

$$\gamma^{(3)}_{\text{hexagonal}} = \tfrac{3}{4}\cos 6\theta[(\mathcal{G}+\mathcal{G}_{111}) - 3\mathcal{G}_{112} + 2\mathcal{G}_{123}] \equiv \mathcal{H}_\alpha \cos 6\theta. \tag{25}$$

Note that the validity of the formulas up to Eq. (23) is not limited to any particular lattice. It is also straightforward to verify that for fcc, this correction is a linear combination of a constant term, $K_{4,1}(\theta,\varphi)$, and $K_{6,1}(\theta,\varphi)$. Nevertheless, we focus on the energy corrections for the 2D hexagonal lattice

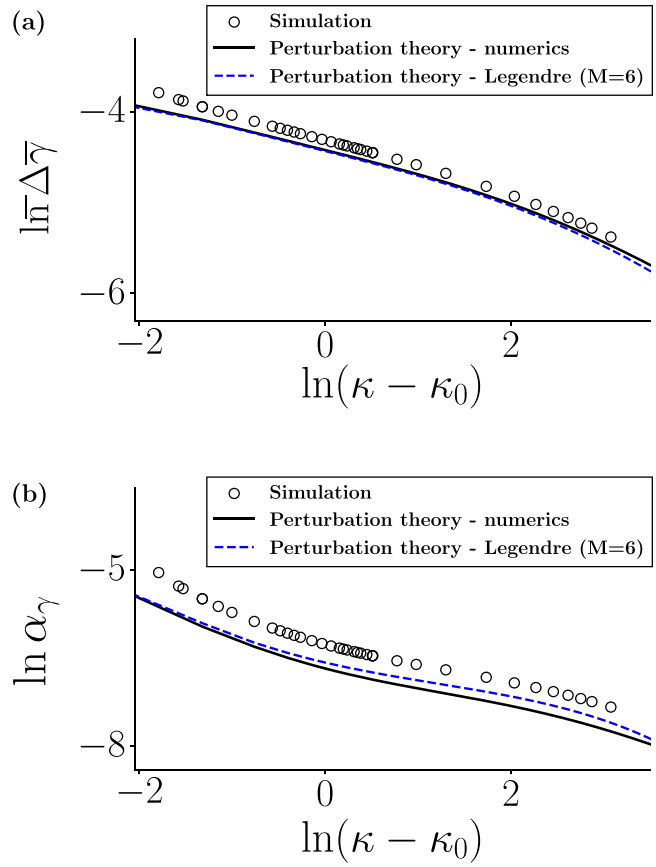

FIG. 3. (a) The anisotropy parameter and (b) the energy offset of hexagonal lattices according to Eqs. (20) and (23) are compared with simulations (open circles). Here, $\kappa_0 = -\frac{5}{3}$ refers to the lower limit of κ due to the stability of the double-well potential discussed in Appendix A.

predicted by Eqs. (20) and (23), with the isotropic profile and energy being

$$\psi^{(0)}(\xi) = \frac{1}{2}\left(1+\tanh\frac{\xi}{\sqrt{2}}\right),$$
$$\gamma^{(0)} = \frac{\sqrt{2}}{2}, \tag{26}$$

and a quantitative comparison can be made between the generalized GL theory, the perturbation solution, and the PFC model. The corresponding anisotropy parameter and energy offset are $\alpha_\gamma = \mathcal{H}_\alpha(\kappa)/[\gamma^{(0)}+\gamma^{(2)}(\kappa)]$ and $\Delta\bar{\gamma} = \gamma^{(2)}(\kappa)$, respectively. Figure 3 plots how α_γ and $\Delta\bar{\gamma}$ change with κ for hexagonal lattices predicted by the perturbation theory alongside results extracted from simulations of coupled differential equations (8). The simulation results and the perturbation theory are in good agreement that both anisotropy and energy offset diminish when the coupling κ becomes stronger. The analytical expressions that show the explicit dependence of α_γ and $\Delta\bar{\gamma}$ on κ for hexagonal lattices can be obtained using the associated Legendre polynomials as detailed in Appendix C.

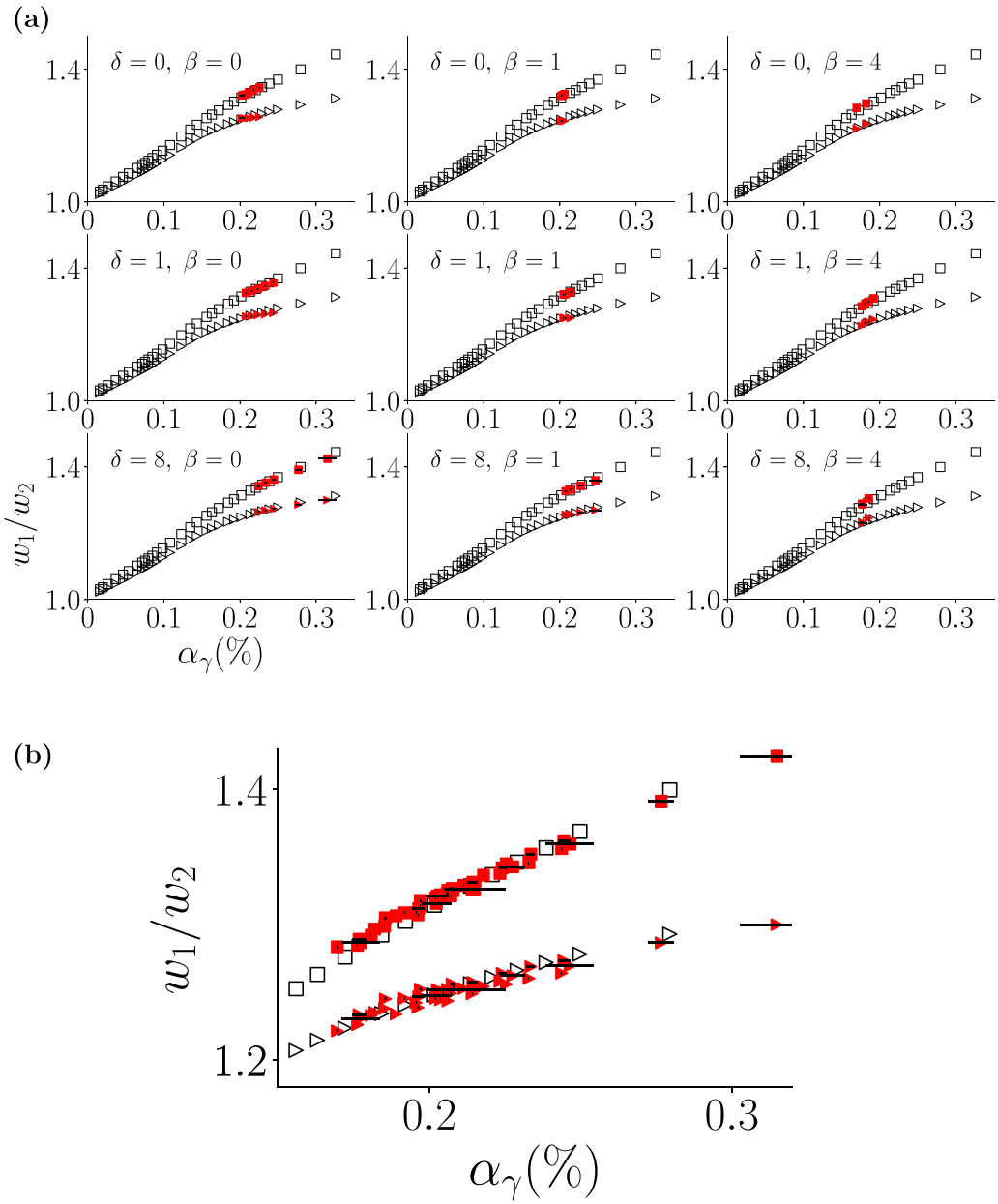

FIG. 4. (a) Graphs of w_1/w_2 ratios vs interfacial energy anisotropy for the GL theory (open symbols) and PFC simulations with different combinations of $(\epsilon, \delta, \beta)$ (solid symbols). The upper branch (squares) shows w_1/w_2 at $\theta = 0$, while the lower branch (triangles) corresponds to $\theta = \pi/6$. Within each plot, δ and β are fixed at a set of values taken between (0,0) and (8,4). The PFC data from all nine plots are overlaid to yield (b).

V. UNIVERSAL SURFACE ANISOTROPY

The connection between the present model and other approaches, such as MD simulations or PFC calculations, can be drawn by relating one dimensionless quantity predicted by the GL theory to another. In particular, the anisotropy parameter α_γ and the ratio of the interface widths of amplitude profiles corresponding to different principal RLVs are determined uniquely once the free-energy landscape is specified (e.g., coupling strength κ in the hexagonal lattice model). The PFC model has been used widely in modeling interfaces in materials on the atomistic scale in and out of equilibrium [47–59], and it has been shown to exhibit a close relation to classical DFT [60–65]. In the diffusive interface limit, the solid density in the PFC model can be well approximated by the summation of density waves of principal RLVs. Therefore, as a way to validate the GL theory, we compare the relation between said dimensionless quantities predicted by the GL theory for the hexagonal lattice with that of PFC simulations.

To be more specific, given a density amplitude profile $\psi_i(\xi)$ across the solid-liquid interface, we define the interface width w_i as the value of w that minimizes

$$\int d\xi \left[\psi_i(\xi) - \frac{1 + \tanh[(\xi - \xi')/w]}{2}\right]^2, \tag{27}$$

where ξ' takes into account the spatial shift of simulated profiles and is also chosen so that the above expression is minimized. There then exists, according to the GL theory, a one-to-one correspondence between α_γ and the ratio w_1/w_2 at any given θ. To demonstrate the applicability of the present theory, we consider here an extension to the original PFC model of which the free-energy functional is

$$F[\psi] = \int d\mathbf{r}\left[\frac{1}{2}\psi[-\epsilon + (1+\nabla)^2 - \delta(\nabla^2 + 2\nabla^4 + \nabla^6)]\psi + \frac{\psi^4}{4} + \beta\frac{\psi^6}{6}\right]. \tag{28}$$

Equation (28) is obtained by considering a simple generalization of the PFC kernel and nonlinear terms under the condition that the characteristic wave number at $k = 1$ be preserved. The parameter δ therefore only alters the second derivative of $C(k)$ at $k = 1$, resulting in variable interface widths.

In Fig. 4, the interface width ratios w_1/w_2 at $\theta = 0^\circ$ and 30° are plotted against α_γ for both GL theory and PFC simulations. As discussed in Sec. III, as κ increases, the profiles of different principal RLVs tend to attract each other more strongly, resulting in similar profiles. This picture is once again rendered appropriate when one observes that in Fig. 4, $w_1/w_2 \to 1$ as α_γ approaches 0 (i.e., the isotropic limit). Furthermore, Fig. 4 also shows that the PFC results and those predicted by the GL theory agree well in spite of different combinations of parameters $(\epsilon, \delta, \beta)$ employed in the PFC and varying interface widths. This agreement is observed when $\epsilon \lesssim 0.1$ at $\delta = 0$, where the one-mode approximation holds well [22], with the condition being less restrictive as δ gets larger. The universal relation between α_γ and the ratio w_1/w_2 observed in the PFC suggests that the solid-liquid surface energy anisotropy can be well described by the GL theory given that the underlying lattice can be approximated by its principal RLVs. Moreover, with the anisotropy α_γ measured from the PFC, one immediately determines its corresponding κ value in the GL theory; see Fig. 1(b). Note that in the limit of diffusive interfaces the anisotropy does not depend on the interface width. However, this discrepancy is to be expected as the interface width becomes comparable to the lattice spacing, in which case the interface would no longer be diffusive and the analyses found in Refs. [42,43] would be appropriate.

VI. CONCLUSIONS AND DISCUSSION

We employed the GL theory, which has its roots in the classical DFT of freezing, to reveal explicitly how the lattice symmetry at the atomistic level dictates surface energy anisotropy at the macroscopic level through a perturbative framework. The order parameters considered in the GL theory are the amplitudes of density waves corresponding to the principal RLVs, whose profiles are generally anisotropic as a result of discrete rotational symmetry of lattices. The proposed perturbation scheme treats the isotropic density waves as the unperturbed state, with the anisotropic deviations in squared-gradient coefficients serving as perturbing parameters. We show systematically that depending on the lattice symmetry, the surface energy anisotropy appears at the corresponding order of the perturbative expansion. For example, square lattices and fcc lattices exhibit fourfold and cubic symmetry, respectively, in surface energy anisotropy at $\gamma^{(2)}$, while hexagonal lattices exhibit sixfold symmetry at $\gamma^{(3)}$.

Our results are general in the sense that the analytical derivation of the anisotropy, which results in Eqs. (19), (20), and (23), is applicable to any interface orientation (and any lattice symmetry) and does not rely on assumptions of the functional form of the profiles. In addition, we show that the magnitude of the anisotropy can be analytically linked to the shape of the double-well potential, which is closely related to the interatomic potential or the pair correlation function of materials. As an example, we show that due to its symmetry, the free-energy functional for hexagonal lattices, considering up to quartic terms, can be parametrized by only a single parameter. This parameter is shown to play the role of coupling density waves of different RLVs in an attractive manner, hence reducing anisotropy when increased. Straightforwardly, a correspondence between the shape of the free-energy landscape and surface energy anisotropy for other lattice structures can be drawn in a similar fashion. It is of interest to note that the shown dependence of surface energy anisotropy on the shape of the free-energy landscape provides a possible alternative way of modeling solidification using the phase-field approach: The material-dependent anisotropy can be mapped to different free-energy landscapes depending on materials, which naturally gives rise to anisotropic surface properties and crystal growth morphology.

Since the lattice symmetry and the shape of the free-energy landscape unilaterally determine the order parameter profiles across the solid-liquid interfaces, which gives rise to the surface energy anisotropy, a universal relation between dimensionless quantities such as the ratio of profile widths and the anisotropy parameter is expected. A generalized PFC model that includes an additional kernel and nonlinearity is employed to examine the aforementioned relation for hexagon-liquid interfaces in 2D. In spite of different values of parameters and varying interface widths, the PFC results of ratios of density wave widths w_i/w_j and the anisotropy parameter α_γ collapse in accordance with the prediction of the GL theory, validating the universal relation for solid-liquid systems which can be well approximated by principal RLVs.

ACKNOWLEDGMENT

The authors gratefully acknowledge the support of the National Science and Technology Council, Taiwan (Grant No. MOST 111-2112-M-007-024), and the support from the National Center for Theoretical Sciences, Taiwan.

APPENDIX A: CLASSIFICATION OF DOUBLE-WELL POTENTIALS

1. Translational invariance and point-group symmetry

The free-energy functional (5) depends on the $2N$ complex density wave amplitudes $\psi_i(\boldsymbol{\xi})$ corresponding to the principal-mode wave vectors $\mathbf{k}_i$. These transform under spatial translation as

$$\psi_i(\boldsymbol{\xi}) \to \psi_i(\boldsymbol{\xi})e^{i\mathbf{k}_i\cdot\boldsymbol{\xi}}.$$

The potential $V(\boldsymbol{\psi})$ should only consist of terms that respect the translational symmetry, which leads to the following

constraint:

$$\psi_i\psi_j\psi_k\cdots\psi_{i'}^*\psi_{j'}^*\psi_{k'}^*\cdots \text{ is allowed in } V(\boldsymbol{\psi}) \Rightarrow (\mathbf{k}_i+\mathbf{k}_j+\mathbf{k}_k+\cdots)-(\mathbf{k}_{i'}+\mathbf{k}_{j'}+\mathbf{k}_{k'}+\cdots)=0, \tag{A1}$$

which can be seen as a kind of momentum conservation. In d dimensions, under the assumption that the effect of lattice distortion is negligible in the system of interest, we have d degrees of freedom (DOFs) to arbitrarily shift the origin of the plane waves to make ψ_i real, leaving us to $2N-d$ real degrees of freedom for the profiles. However, the absolute magnitudes of the profiles $|\psi_i|=|\psi_i^*|$ only contribute N DOFs, meaning that $N-d$ phases cannot be removed by a shift of origin. So, for example, for a hexagonal lattice the potential in general takes the form $V(|\psi_1(\mathbf{r})|, |\psi_2(\mathbf{r})|, |\psi_3(\mathbf{r})|, \varphi)$, where φ represents an irremovable phase which can be (arbitrarily) chosen by letting $\psi_i(\mathbf{r})=|\psi_i|e^{i\varphi}$, while for a square lattice $V(\psi_1,\psi_2)$ is sufficient.

On the other hand, $V(\boldsymbol{\psi})$ also has to respect the discrete point-group symmetry imposed by the underlying lattice. After reducing to two DOFs for the square lattice by removing phases, D_4 becomes S_2, implying that $V(\psi_1,\psi_2)$ has to be a symmetric polynomial of ψ_1 and ψ_2. As for the hexagonal lattice, since $\varphi\to-\varphi$ corresponds to spatial rotation by π, only $\cos 3\varphi$, not $\sin 3\varphi$, is allowed in V. Since any polynomial of $\cos 3\varphi$ always has its local minima at $\varphi=0$ or $\varphi=\pi/6$, we can set $\cos 3\varphi=\pm 1$. A term such as $\psi_1\psi_2\psi_3+\psi_1^*\psi_2^*\psi_3^*=2|\psi_1\psi_2\psi_3|\cos 3\varphi$, which is permitted by symmetry, then becomes $\pm 2|\psi_1\psi_2\psi_3|$. The resulting V will then be a symmetric polynomial of ψ_1, ψ_2, and ψ_3. The simplest polynomial double-well potentials for relevant lattices are listed below (here, ψ_i is used in place of $|\psi_i|$).

Square:

$$V=\sum_i\left(\psi_i^6-2\psi_i^4+\psi_i^2\right)+\kappa\left(\psi_1^4+\psi_2^4-2\psi_1^2\psi_2^2\right)+\kappa'\left(\psi_1^6+\psi_2^6-\psi_1^4\psi_2^2-\psi_1^2\psi_2^4\right).$$

Hexagonal:

$$V=\sum_i\left(\psi_i^4+\psi_i^2\right)-6\psi_1\psi_2\psi_3+\kappa\left(\psi_1^4+\psi_2^4+\psi_3^4-\psi_1^2\psi_2^2-\psi_1^2\psi_3^2-\psi_2^2\psi_3^2\right).$$

fcc:

$$\begin{aligned}V=&\sum_i\left(\psi_i^6-2\psi_i^4+\psi_i^2\right)+\kappa\left(\sum_i\psi_i^4-\frac{2}{3}\sum_{\text{sym}}\psi_1^2\psi_2^2\right)+\kappa'\left(\sum_i\psi_i^4-4\psi_1\psi_2\psi_3\psi_4\right)\\&+\kappa''\left(\sum_i\psi_i^6-\psi_1\psi_2\psi_3\psi_4\sum_i\psi_i^2\right)+\kappa'''\left(\sum_i\psi_i^6-\sum_{\text{sym}}\psi_1^2\psi_2^2\psi_3^2\right)+\kappa''''\left(\sum_i\psi_i^6-\frac{1}{3}\sum_{\text{sym}}\psi_1^4\psi_2^2\right).\end{aligned} \tag{A2}$$

2. Stability of the hexagonal lattice double-well potential

The stability of the free-energy landscape requires that the Hessian matrix of V at the liquid and solid minima be positive definite. The former, which corresponds to $\psi_i=0$, is automatically satisfied by the potentials shown in (A2). On the solid side where $\psi_i=1$, this condition leads to a nontrivial constraint on the coupling constants. For hexagonal lattices, the Hessian matrix is

$$\mathbf{H}(\kappa)=\begin{pmatrix}14+8\kappa & -6-4\kappa & -6-4\kappa\\ -6-4\kappa & 14+8\kappa & -6-4\kappa\\ -6-4\kappa & -6-4\kappa & 14+8\kappa\end{pmatrix},$$

whose principal minors have zeros at $\kappa=-\frac{5}{3}$, $-\frac{7}{4}$, and -2, implying that the coupling constant κ is subject to a lower bound:

$$\kappa>\kappa_0\equiv-\tfrac{5}{3}. \tag{A3}$$

APPENDIX B: GENERAL FUNCTIONAL PERTURBATION THEORY

The general framework of perturbative calculations for minimizing an energy functional $\gamma[\psi_i(\xi)]$ is presented here. In particular, the expressions for corrections to energy up to the third order are discussed, as well as the governing equations obeyed by the fields up to the second order. The free-energy functional is decomposed into the sum of a solvable part γ_0 and a small deviation from it, which is denoted by γ_1:

$$\gamma[\boldsymbol{\psi}(\xi)]=\gamma_0[\boldsymbol{\psi}(\xi)]+\epsilon\gamma_1[\boldsymbol{\psi}(\xi)], \tag{B1}$$

where ϵ is a dummy parameter for keeping track of the order during expansions and is set to unity in the end. The validity of this approach is then justified by the smallness of γ_1 itself, rather than that of ϵ. Assume that the fields are expanded as a power series of ϵ:

$$\psi_i=\sum_p\epsilon^p\psi_i^{(p)}. \tag{B2}$$

The energy functional is then readily expanded order by order. Specifically, γ_0 and γ_1 are expanded up to $O(\epsilon^3)$ and $O(\epsilon^2)$, respectively. For simplicity, we introduce a concise notation where $\gamma_0\equiv\gamma_0[\psi^{(0)}]$, $\Delta_i\gamma_0\equiv[\delta\gamma_0/\delta\psi_i(\xi)][\psi^{(0)}]$, and $\Delta_{ij}^2\gamma_0\cdot\psi_j^{(1)}\equiv\int d\zeta\ \psi_j^{(1)}(\zeta)\cdot\delta^2\gamma_0[\psi^{(0)}]/\delta\psi_i(\xi)\delta\psi_j(\zeta)$, etc. Note that repeated indices imply a summation over all

possible values of the index. We obtain

$$\begin{aligned}\gamma_0[\psi] &= \gamma_0 + \epsilon\Delta_i\gamma_0\cdot\psi_i^{(1)} + \epsilon^2\Delta_i\gamma_0\cdot\psi_i^{(2)} \\ &\quad + \frac{\epsilon^2}{2}\Delta_{ij}^2\gamma_0\cdot\psi_i^{(1)}\psi_j^{(1)} \\ &\quad + \epsilon^3\Delta_i\gamma_0\cdot\psi_i^{(3)} + \epsilon^3\Delta_{ij}^2\gamma_0\cdot\psi_i^{(1)}\psi_j^{(2)} \\ &\quad + \frac{\epsilon^3}{6}\Delta_{ijk}^3\gamma_0\cdot\psi_i^{(1)}\psi_j^{(1)}\psi_k^{(1)}, \\ \gamma_1[\psi] &= \gamma_1 + \epsilon\Delta_i\gamma_1\cdot\psi_i^{(1)} + \epsilon^2\Delta_i\gamma_1\cdot\psi_i^{(2)} \\ &\quad + \frac{\epsilon^2}{2}\Delta_{ij}^2\gamma_1\cdot\psi_i^{(1)}\psi_j^{(1)}. \end{aligned} \tag{B3}$$

The governing equations for $\psi_i^{(p)}$ are obtained by requiring the energy to be minimized. That is, we take the functional derivative of $\gamma = \gamma_0 + \epsilon\gamma_1$ with respect to ψ_i's and set them to zero. Arranging this equation order by order, we obtain

$$\begin{aligned}&\epsilon^0\text{:}\quad \Delta_i\gamma_0 = 0, \\ &\epsilon^1\text{:}\quad \Delta_{ij}^2\gamma_0\cdot\psi_j^{(1)} + \Delta_i\gamma_1 = 0, \\ &\epsilon^2\text{:}\quad \Delta_{ij}^2\gamma_0\cdot\psi_j^{(2)} + \tfrac{1}{2}\Delta_{ijk}^3\gamma_0\cdot\psi_j^{(1)}\psi_k^{(1)} + \Delta_{ij}^2\gamma_1\cdot\psi_j^{(1)} = 0. \end{aligned} \tag{B4}$$

The minimized energy itself can also be expressed as $\gamma = \sum_p \epsilon^p\gamma^{(p)}$. Evidently, $\gamma^{(0)} = \gamma_0[\psi^{(0)}]$. The first-order energy correction is $\gamma^{(1)} = \Delta_i\gamma_0\cdot\psi_i^{(1)} + \gamma_1[\boldsymbol{\psi}^{(0)}]$, where the first term vanishes since the fields $\psi_i^{(0)}$ must satisfy the zeroth-order governing equations, leaving

$$\gamma^{(1)} = \gamma_1[\psi^{(0)}]. \tag{B5}$$

Similarly, the expressions for $\gamma^{(2)}$ and $\gamma^{(3)}$ are found using Eq. (B3). The results are

$$\begin{aligned}\gamma^{(2)} &= -\tfrac{1}{2}\Delta_{ij}^2\gamma_0\cdot\psi_i^{(1)}\psi_j^{(1)}, \\ \gamma^{(3)} &= \tfrac{1}{6}\Delta_{ijk}\gamma_0\cdot\psi_i^{(1)}\psi_j^{(1)}\psi_k^{(1)} + \tfrac{1}{2}\Delta_{ij}^2\gamma_1\cdot\psi_i^{(1)}\psi_j^{(1)}. \end{aligned} \tag{B6}$$

APPENDIX C: LEGENDRE EXPANSION FOR A HEXAGONAL LATTICE

Evaluating Eqs. (20) and (23) amounts to finding a suitable approximate method to invert the functional operator $\hat{K}$, which can be greatly simplified by projecting it onto a set of orthonormal basis. A natural and straightforward choice would be its own eigenbasis; however, since $\hat{K}$ is equivalent to a Pöschl-Teller Hamiltonian, whose spectrum consists of discrete bound states and a scattering continuum [66], which is analytically formidable to work with, another set of basis functions may be more appropriate. Due to the nature of the operator, it is convenient to use a subset of the associated Legendre polynomials projected from their original defining domain $[-1, 1]$ onto the real space $(-\infty, \infty)$. Specifically, the functions $P_{lm}(y)$ with fixed m form a complete orthogonal basis on $y \in [-1, 1]$. For our purpose, $m = 1$ would be appropriate, as will become apparent in the following passages.

Mapping $y = \tanh\xi$ and taking into account the change of integral measure $dy = \operatorname{sech}^2\xi\, d\xi$, one can define a set of orthonormal functions on the interval $(-\infty, \infty)$:

$$f_l(x) \equiv \frac{\operatorname{sech} x}{\sqrt{C_l}} P_{l1}(\tanh x), \quad C_l \equiv \frac{2(l+1)!}{(2l+1)(l-1)!}, \tag{C1}$$

where $P_{lm}(y)$ are the associated Legendre polynomials, given by the Rodrigues formula $P_{lm}(y) = (-1)^m(1-y^2)^{m/2}\partial_y^{l+m}(y^2-1)^l/2^l l!$. The orthonormality $\langle f_l|f_k\rangle = \delta_{lk}$ then follows. $\chi \equiv \hat{K}^{-1}\varphi$ can then be rewritten as $\chi_l = (K^{-1})_{lk}(\partial^2\psi)_k$, where $\chi_l = \langle f_l|\chi\rangle$ and $K_{lk} = \langle f_l|\hat{K}|f_k\rangle$, etc. With the use of recurrence formulas [67], we obtain the general expression for K_{lk}:

$$\begin{aligned} K_{lk} &= \left\{\frac{1}{(2k-1)(2k+3)}[2k(k+1)(k^2+k-1)\right. \\ &\quad \left. + (2k^2+2k-3)(6+6\kappa)] + 16 + 6\kappa\right\}\delta_{lk} \\ &\quad + \left\{\frac{1}{2k+3}\sqrt{\frac{k(k+1)(k+2)(k+3)}{(2k+1)(2k+5)}}\right. \\ &\quad \times [(6+6\kappa) - (k+1)(k+2)]\delta_{l,k+2} \\ &\quad \left. + 2(9+6\kappa)\sqrt{\frac{k(k+2)}{(2k+1)(2k+3)}}\delta_{l,k+1} + \text{H.c.}\right\}, \end{aligned} \tag{C2}$$

where H.c. denotes matrix transposition. The advantage of this choice of basis is manifest when one notes that $\partial^2\psi^{(0)} \propto f_2(x)$, and so $\langle\psi^{(0)}|\partial^2\hat{K}^{-1}\partial^2|\psi^{(0)}\rangle$ is simply $\langle\psi^{(0)}\partial^2|\partial^2\psi^{(0)}\rangle\,(K^{-1})_{22}$. With Eq. (C2), the energy corrections (20) and (23), using a finite number of basis functions, can be written as explicit functions of κ. In general, they take the form

$$\gamma^{(n)} = \frac{q_n(\kappa)}{p_n(\kappa)},$$

where $p(\kappa)$ and $q(\kappa)$ are polynomials of κ. For example, the second-order energy correction $\gamma^{(2)}$, retaining only three modes, takes the form

$$\sqrt{2}\gamma^{(2)} \approx -\frac{7(36\kappa^2+196\kappa+259)}{400(6\kappa^3+85\kappa^2+315\kappa+336)}.$$

As shown in Fig. 3, with truncation after six basis functions, the energy corrections are very close to those obtained by numerical evaluation of Eqs. (20) and (23).

[1] J. W. Gibbs, *The Collected Works of J. Willard Gibbs* (Yale University Press, New Haven, 1948).
[2] M. Glicksman and N. Singh, J. Cryst. Growth **98**, 277 (1989).
[3] J. Hoyt, M. Asta, T. Haxhimali, A. Karma, R. Napolitano, R. Trivedi, B. Laird, and J. Morris, MRS Bull. **29**, 935 (2004).
[4] J. Friedli, J. L. Fife, P. Di Napoli, and M. Rappaz, Metall. Mater. Trans. A **44**, 5522 (2013).

[5] L. Wang, J. J. Hoyt, N. Wang, N. Provatas, and C. W. Sinclair, Nat. Commun. **11**, 724 (2020).

[6] G. B. McFadden, A. A. Wheeler, R. J. Braun, S. R. Coriell, and R. F. Sekerka, Phys. Rev. E **48**, 2016 (1993).

[7] A. Karma and W.-J. Rappel, Phys. Rev. E **53**, R3017 (1996).

[8] N. Provatas, N. Goldenfeld, and J. Dantzig, Phys. Rev. Lett. **80**, 3308 (1998).

[9] T. Haxhimali, A. Karma, F. Gonzales, and M. Rappaz, Nat. Mater. **5**, 660 (2006).

[10] J. A. Dantzig, P. Di Napoli, J. Friedli, and M. Rappaz, Metall. Mater. Trans. A **44**, 5532 (2013).

[11] O. Tschukin, A. Silberzahn, M. Selzer, P. G. K. Amos, D. Schneider, and B. Nestler, Geotherm. Energy **5**, 19 (2017).

[12] A. Roy and M. P. Gururajan, Cryst. Growth Des. **21**, 1591 (2021).

[13] J. J. Hoyt, M. Asta, and A. Karma, Phys. Rev. Lett. **86**, 5530 (2001).

[14] J. J. Hoyt, M. Asta, and A. Karma, Mater. Sci. Eng.: R: Rep. **41**, 121 (2003).

[15] D. Y. Sun, M. Asta, J. J. Hoyt, M. I. Mendelev, and D. J. Srolovitz, Phys. Rev. B **69**, 020102(R) (2004).

[16] D. Y. Sun, M. Asta, and J. J. Hoyt, Phys. Rev. B **69**, 174103 (2004).

[17] R. L. Davidchack and B. B. Laird, Phys. Rev. Lett. **94**, 086102 (2005).

[18] B. B. Laird and R. L. Davidchack, J. Phys. Chem. B **109**, 17802 (2005).

[19] W. H. Shih, Z. Q. Wang, X. C. Zeng, and D. Stroud, Phys. Rev. A **35**, 2611 (1987).

[20] K.-A. Wu, A. Karma, J. J. Hoyt, and M. Asta, Phys. Rev. B **73**, 094101 (2006).

[21] S. Majaniemi and N. Provatas, Phys. Rev. E **79**, 011607 (2009).

[22] G. I. Tóth and N. Provatas, Phys. Rev. B **90**, 104101 (2014).

[23] T. V. Ramakrishnan and M. Yussouff, Phys. Rev. B **19**, 2775 (1979).

[24] A. D. J. Haymet and D. W. Oxtoby, J. Chem. Phys. **74**, 2559 (1981).

[25] D. W. Oxtoby and A. D. J. Haymet, J. Chem. Phys. **76**, 6262 (1982).

[26] W. A. Curtin, Phys. Rev. Lett. **59**, 1228 (1987).

[27] B. B. Laird, J. D. McCoy, and A. D. J. Haymet, J. Chem. Phys. **87**, 5449 (1987).

[28] K.-A. Wu, C.-H. Wang, J. J. Hoyt, and A. Karma, Phys. Rev. B **91**, 014107 (2015).

[29] A. Jaatinen, C. V. Achim, K. R. Elder, and T. Ala-Nissila, Phys. Rev. E **80**, 031602 (2009).

[30] K.-A. Wu, A. Adland, and A. Karma, Phys. Rev. E **81**, 061601 (2010).

[31] K.-A. Wu, S.-C. Lin, and A. Karma, Phys. Rev. B **93**, 054114 (2016).

[32] A. Nourian-Avval and E. Asadi, Comput. Mater. Sci. **128**, 294 (2017).

[33] S. Kumar, M.-W. Liu, K.-A. Wu, and M. Gururajan, Comput. Mater. Sci. **202**, 110982 (2022).

[34] P. Galenko, F. I. Sanches, and K. Elder, Physica D (Amsterdam) **308**, 1 (2015).

[35] V. Ankudinov, K. R. Elder, and P. K. Galenko, Phys. Rev. E **102**, 062802 (2020).

[36] N. Ofori-Opoku, J. A. Warren, and P. W. Voorhees, Phys. Rev. Mater. **2**, 083404 (2018).

[37] N. Goldenfeld, B. P. Athreya, and J. A. Dantzig, Phys. Rev. E **72**, 020601(R) (2005).

[38] K. R. Elder, Z.-F. Huang, and N. Provatas, Phys. Rev. E **81**, 011602 (2010).

[39] M. Salvalaglio and K. R. Elder, Modell. Simul. Mater. Sci. Eng. **30**, 053001 (2022).

[40] A. D. J. Haymet and D. W. Oxtoby, J. Chem. Phys. **84**, 1769 (1986).

[41] F. Spaepen, Acta Metall. **23**, 729 (1975).

[42] Z.-F. Huang, Phys. Rev. E **87**, 012401 (2013).

[43] Z.-F. Huang, Phys. Rev. E **93**, 022803 (2016).

[44] R. L. Davidchack and B. B. Laird, J. Chem. Phys. **108**, 9452 (1998).

[45] M.-W. Liu and K.-A. Wu, Phys. Rev. B **96**, 214106 (2017).

[46] W. R. Fehlner and S. H. Vosko, Can. J. Phys. **54**, 2159 (1976).

[47] K. R. Elder and M. Grant, Phys. Rev. E **70**, 051605 (2004).

[48] J. Berry, K. R. Elder, and M. Grant, Phys. Rev. B **77**, 224114 (2008).

[49] J. Mellenthin, A. Karma, and M. Plapp, Phys. Rev. B **78**, 184110 (2008).

[50] K.-A. Wu and P. W. Voorhees, Phys. Rev. B **80**, 125408 (2009).

[51] L. Gránásy, G. Tegze, G. I. Tóth, and T. Pusztai, Philos. Mag. **91**, 123 (2011).

[52] K.-A. Wu and P. W. Voorhees, Acta Mater. **60**, 407 (2012).

[53] A. J. Archer, M. J. Robbins, U. Thiele, and E. Knobloch, Phys. Rev. E **86**, 031603 (2012).

[54] E. J. Schwalbach, J. A. Warren, K.-A. Wu, and P. W. Voorhees, Phys. Rev. E **88**, 023306 (2013).

[55] S. Tang, Y.-M. Yu, J. Wang, J. Li, Z. Wang, Y. Guo, and Y. Zhou, Phys. Rev. E **89**, 012405 (2014).

[56] S.-C. Lin, M.-W. Liu, M. P. Gururajan, and K.-A. Wu, Acta Mater. **102**, 364 (2016).

[57] M. Salvalaglio, R. Backofen, K. R. Elder, and A. Voigt, Phys. Rev. Mater. **2**, 053804 (2018).

[58] Z.-L. Wang, Z. Liu, Z.-F. Huang, and W. Duan, Phys. Rev. Mater. **4**, 103802 (2020).

[59] M.-W. Liu, M. P. Gururajan, and K.-A. Wu, Phys. Rev. Mater. **6**, 023601 (2022).

[60] K. R. Elder, N. Provatas, J. Berry, P. Stefanovic, and M. Grant, Phys. Rev. B **75**, 064107 (2007).

[61] K.-A. Wu and A. Karma, Phys. Rev. B **76**, 184107 (2007).

[62] Z.-F. Huang, K. R. Elder, and N. Provatas, Phys. Rev. E **82**, 021605 (2010).

[63] E. Alster, K. R. Elder, J. J. Hoyt, and P. W. Voorhees, Phys. Rev. E **95**, 022105 (2017).

[64] A. J. Archer, D. J. Ratliff, A. M. Rucklidge, and P. Subramanian, Phys. Rev. E **100**, 022140 (2019).

[65] Z.-L. Wang, Z. Liu, W. Duan, and Z.-F. Huang, Phys. Rev. E **105**, 044802 (2022).

[66] D. E. Alvarez-Castillo, arXiv:0808.1642.

[67] G. B. Arfken, H. J. Weber, and F. E. Harris, in *Mathematical Methods for Physicists (Seventh Edition)*, 7th ed., edited by G. B. Arfken, H. J. Weber, and F. E. Harris (Academic, Boston, 2013), pp. 715–772.